

Choice of a Turbulence Model for Pump Intakes

A. Škerlavaj^{1*}, L. Škerget², J. Ravnik² and A. Lipej¹

¹ Turboinštitut, Rovšnikova 7, 1210 Ljubljana, Slovenia

² University of Maribor, Faculty of Mechanical Engineering, Smetanova ulica 17, 2000 Maribor, Slovenia

* corresponding author (aljaz.skerlavaj@turboinstitut.si)

Abstract: This paper is focused on the choice of a suitable turbulence model for simulations of an industrial pump's intake, from the perspective of accuracy and, partially, also the CPU time. Twelve steady-state and transient simulations were made on a fine computational mesh, using turbulence models such as: the shear stress transport (SST), the scale-adaptive simulation (SAS), the Reynolds stress model (RSM), the explicit algebraic Reynolds-stress model (EARSM), the detached eddy simulation (DES) and the large eddy simulation (LES). The curvature-correction (CC) option was assessed for the SST and SAS turbulence models. The results were compared with the LES and with published experimental results. Although all the models could predict the main floor vortex, there were still some substantial differences. We were able to conclude that it is better to use either the SST-CC turbulence model, due to its low computational resources and far better results than the SST model, or the SAS-CC turbulence model, since its predictions are quite similar to the LES results. In the final step, good agreement with experimental results was shown for a longer simulation with the SAS-CC turbulence model.

Keywords: Turbulence model, Simulation, CFD, Vortex, Pump Intake, Pump Sump, SAS, LES

1. INTRODUCTION

Pump-intake design has an important role in good pump operation and therefore on the pump having a long lifetime. The design of the intake structures is specified in standards, for instance in [1]. Nevertheless, the model testing of intake structures is still required in cases where the geometry deviates from that recommended or in special cases, as described in [1]. The acceptance criteria for the model tests are based on the uniformity of the flow: the vortices should not have a coherent core, the swirling in the pipe should be low and approximately constant, and the velocities in the pipe should be uniform and constant over time.

Although there were some studies as early as 1989, it can be said that the important computational fluid dynamics (CFD) computations of pump-intake structures only started with [2] and [3], when the numerical model was compared with the experimental model. The numerical simulation was based on a steady-state computation using the k - ϵ turbulence model on a structured computational mesh with 550,000 nodes. The conclusion of [3] was that anisotropic turbulence models and unsteady computations would enhance the prediction of vortices.

In 2000 a first comparison between the k - ϵ and k - ω turbulence models for steady-state computations was conducted [4]. Although there is no comparison with any measurements, the turbulence models themselves showed no major differences in terms of the streamline patterns and vorticity contours. The analysis of the intensity of the vortices showed that k - ϵ and the low-Reynolds-number Wilcox k - ω turbulence model predicted vortices with a similar intensity, whereas the high-Reynolds Wilcox k - ω turbulence model predicted vortices with a slightly lower intensity.

Since 1998, computing power has increased significantly. Nevertheless, most of the reported computations are still being made using the k - ϵ , k - ω or Shear Stress Transport (SST) turbulence models on relatively coarse meshes. The most notable exception is the work of Tokyay and Constantinescu [5], in which the Large Eddy Simulation (LES) and SST turbulence models were compared to the PIV data of a pressurized pump sump (no free surface), measured by Yulin et al. [6]. The steady SST computation using the Fluent commercial software was made on a mesh with approximately 1.5 million cells, and the LES computation was made on a mesh with approximately 5 million cells. The LES model results showed good qualitative and quantitative agreement with the PIV data, while the SST model failed even qualitatively to predict the turbulence kinetic energy of the bottom part of the main floor-attached vortex. In the case of the SST the highest TKE values were reached in the annular-shaped region, instead of in a region along the centerline. The SST qualitative disagreement was, in our opinion, most likely the result of a sparse mesh in the pump-column area.

Since the LES turbulence model is computationally expensive and as such not very suitable for industrial-case computations, we decided to simulate the case of Yulin et al. [6] with several different turbulence models. The question we wanted to answer was which turbulence model was most suitable for industrial needs? In order to eliminate the computational mesh's influence on our results, all the computations were made with the same mesh. The first results [7] indicated that while the transient SST computation seriously under-predicted the turbulence kinetic energy of the floor vortex and proved to be only conditionally acceptable for the vortex prediction, the SAS-SST turbulence model gave approximately the same results as the LES.

The current work is a continuation of [7]. The results of 11 simulations using six different turbulence models and some of their variants are compared to our LES computation and to measurements published in [5]. The main question is which turbulence model can be used for industrial simulations of the intake structures in order to relatively accurately capture the important flow phenomena? The paper concentrates on the floor vortex, since in our opinion all the anomalies in the flow would eventually be visible in the bell area. In the second part of the paper, the longer SAS-CC turbulence-model simulation is compared to the measurement data.

2. DISCUSSION ABOUT TURBULENCE MODELS

In this paper an isothermal flow of an incompressible Newtonian viscous fluid with constant material properties was assumed; this can be described by the following continuity and momentum Navier-Stokes equations:

$$\nabla \cdot \mathbf{u} = 0, \quad (1)$$

$$\frac{\partial \mathbf{u}}{\partial t} + (\mathbf{u} \cdot \nabla) \mathbf{u} = -\frac{1}{\rho_0} \nabla p + \nu_0 \nabla^2 \mathbf{u}. \quad (2)$$

As a direct numerical simulation (DNS), which solves the above equations directly without the use of any turbulence model, is extremely computationally expensive for simulations of turbulent flows, the above equations are usually substituted by Reynolds averaged equations and closed by additional closure assumptions (called turbulence models), or filtered in the case of the LES.

Each year's progress in computational capabilities makes it possible to use computationally more demanding turbulence models in the CFD computations. At the moment, the general usage of turbulence models spans the range from two-equation linear eddy-viscosity Reynolds-averaged Navier–Stokes (RANS) based models, such as the k - ε or k - ω models, to more demanding RANS models, such as the Reynolds Stress Models (RSM), or even to the LES turbulence models.

For a CFD computation, the computational cost is a result of the turbulence model, the computational mesh and the computation time step used. The turbulence model, the mesh and the time step are interconnected. The usage of a more demanding turbulence model generally requires finer meshes and shorter time steps. If they are suitable for a specific case, two-equation, linear turbulence models are preferred because of their low computational cost.

One of the most often used two-equation turbulence models in Ansys CFX [8] is the SST turbulence model [9]. It is a combination of the k - ε and k - ω models, with the k - ε model being used in the free-stream zone and the k - ω model being used near the wall, thus providing us with the best of both models. The SST also limits the eddy-viscosity. Although the SST model can predict the separation point quite well, the flow recovery is too slow and the separation area may become too large ([9], [10], [11] and [12]).

If two-equation models cannot give satisfactory results for a particular case, one is confronted with the choice of computationally more expensive models. RSM models solve seven additional transport equations for 3-dimensional flows instead of two, as do the two-equation models, and this makes these models much more computationally expensive. A good point of the RSM models is that the Reynolds stresses are computed directly and can therefore predict the anisotropic turbulence. Nevertheless, even the use of RSM models might not prevent a CFD user from incorrectly estimating the turbulent mixing in a separated shear layer and hence over-predicting the extent of a separated region [13]. Another well-known problem of the RSM models is their numerical instability.

In order to simplify the computationally expensive RSM models, explicit algebraic Reynolds-stress models (EARSMS) have been derived from them. As stated in [14], the EARSMS model is up to 10 percent more expensive per iteration than the two-equation models. It has been shown in the case of a convexly curved 2-dimensional boundary layer that the performance of the basic EARSMS model (without a curvature-correction term) is better than the performance of the linear eddy viscosity models. It was also shown that by using a curvature correction their solution is closer to the RSM solution.

As the previously mentioned two-equation models are not capable of capturing the effects of streamline curvature and system rotation, it has been suggested by Spalart and Shur [15] that the curvature-correction term be implemented into these models. The modified SST model [16], denoted as SST-CC, is described as being much

more accurate than the SST over a wide range of flows and quite competitive with the RSM in terms of accuracy. It is also computationally robust and efficient, increasing the CPU time per iteration by only 1%.

The LES turbulence model is known to be computationally very expensive compared to the two-equation turbulence models. As the LES model is based on filtering the flow into small isotropic and large anisotropic vortices, the mesh elements should be relatively small to model the vortices correctly. Nevertheless, the main reason for the large number of mesh elements in a “true” LES comes from a boundary-layer, mesh-resolution requirement. Along with the denser meshes, small time steps with a Courant number of less than 1 are needed, which makes the overall computation much more computationally expensive than the one with the SST model. The third reason that makes the LES inappropriate for industrial cases is the inlet boundary-condition treatment. In LES the turbulence at the inlet surface cannot be specified by the equation parameters, such as k and ϵ . It can only be simulated by another LES computation, in which the turbulent structures are formed from the wall boundary layer.

The strict demands of a correct LES simulation have given rise to numerous hybrid turbulence models in the past few years. In the current paper we concentrate on the Detached Eddy Simulation (DES) model, which is an interfacing RANS and LES model using the Fröhlich and Terzi [17] classification, and on the Scale-Adaptive-Simulation (SAS) SST model, which is a so-called second-generation URANS model using the same classification.

In the DES model [18], a RANS model is used at the boundary layer and a LES model in detached regions. The detachment point for the first version of the DES was sensitive to the mesh size. In [9], an SST turbulence model was chosen for the RANS part of the DES. By modifying the dissipation term in the k equation of the SST model, as shown in [9], the detachment point of the SST-DES is not sensitive to the mesh size. In the later version of the DES, called the delayed DES (DDES) [19], a similar modification was made, which allows the DES to be used with other RANS models. Like the LES models, the DES also requires small time steps with a Courant number of less than 1.

The SAS-SST model ([20] and [21]) is an improved, unsteady RANS method that develops LES-like solutions in unstable flow regimes. It is an SST model with an additional production term in the ω equation, which increases when the flow equations start to become unsteady. The increase in the SAS term results in a slower decay rate of the Reynolds stresses due to the smaller turbulent viscosity ([22]). The model was born from the revised Rotta's k - kL turbulence model, which included an integral length scale L into the turbulence-dissipation equation. The detailed development of the SAS model from the revised k - kL model can be found in [23], whereas its inclusion in the SST model is thoroughly described in [21]. Nevertheless, it is important to note that the main difference between the other two-equation models and the SAS is the ability of the SAS to resolve turbulence scales due to the introduction of the von Karman length scale. An important feature that distinguishes it from the LES and DES solutions is the fact that if the turbulence scales cannot be resolved due to a time step larger than the Courant number 1, the eddy viscosity is adjusted accordingly, up to the steady RANS solution. As in the case of the DES, the boundary layer for the SAS-SST is treated in the RANS mode.

The decision about a suitable turbulence model chosen in a CFD computation is not easy. Test cases are important, either experimental or highly resolved numerical data (LES or even DNS), as for instance in [13]. In order to decide on an appropriate turbulence model for a pump-sump case, the turbulence models are compared to the experimental results by Yulin et al. [6], published in the works of Tokyay and Constantinescu ([5] and [24]), and also to our LES computation of the selected case.

3. DESCRIPTION OF THE INTAKE MODEL AND THE COMPUTATIONAL MESH

The geometry of a pump sump's numerical model (Fig. 1, Table 1), which is based on the experimental model [6], was precisely described in [24].

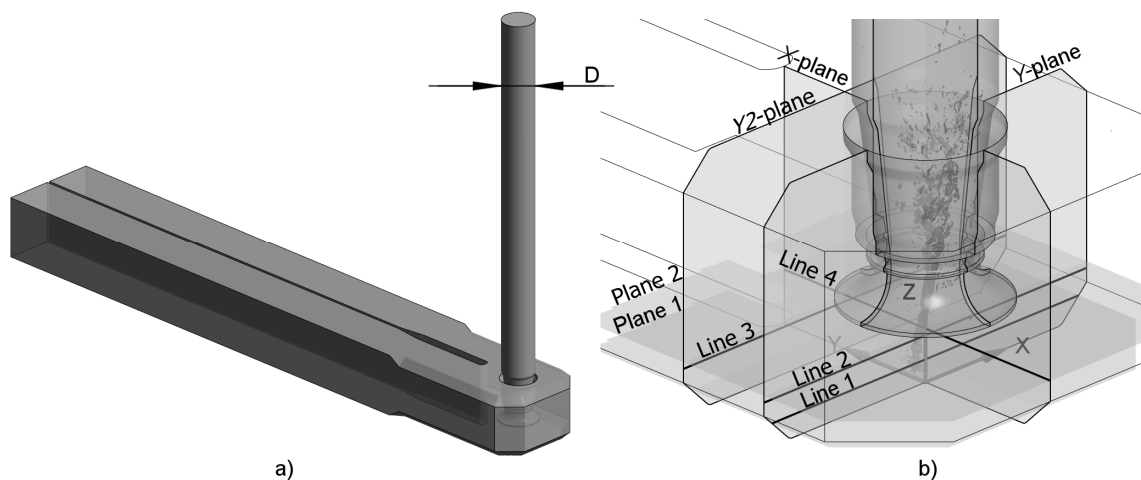


Fig. 1. Geometry of a pump-sump test-case model: a) whole computational domain; b) detailed view with formed main floor vortex in pump-bell region, coordinate system, X-plane, Y-plane, Y2-plane ($0.77D$ from Y-plane), Plane 1 at $Z=0.17D$, Plane 2 at $Z=0.40D$, Line 1 (cross-section of Plane 1 and Y-plane), Line 2 (in Y-plane at $Z=0.35D$), Line 3 (in Y2-plane at $Z=0.35D$) and Line 4 (cross-section of Plane 2 and X-plane).

Table 1. Characteristic geometry dimensions of the computed pump sump.

Outlet pipe diameter D	129.8 mm
Pump sump height	$1.91D$
Inlet channels width	$1.49D$
Bell mouth maximum diameter	$1.23D$
Bell mouth distance from floor	$0.62D$
Peer to pipe center distance	$1.35D$
Simulated pump column height	$12.8D$
Simulated pump sump model length	$20.5D$

The inlet section is divided into two channels with unequal discharges, 0.905 and 0.385 m^3/min . Water flows through the channels, mixes, enters the pump column through the pump bell, and exits through the outlet at the top of the pump column. Due to the non-equal, inlet-flow rate a strong floor vortex is formed in the pump-bell area. For the computation purposes, in order to obtain good inlet- and outlet-velocity profile approximations, the two inlets were moved upstream and the outlet moved further downstream. This results in a pump-sump model length of $20.5D$ instead of $7.7D$ and a pump-column length above the surface of $12.8D$ instead of approximately $2D$, as in [5].

In order to eliminate the influence of the mesh on our results, a fine computational mesh was created and various turbulence models were tested on the same computational mesh. The mesh is a bit denser than the one in [5], which has already produced good results in the case of an LES simulation. Therefore, the mesh is expected to be fine enough for all the tested turbulence models. A structured mesh with approximately 35 million nodes was created (Fig. 2). The mesh has more elements than the one in [5] due to its longer inlet section (7.5 million elements), longer outlet section (7.5 million elements) and higher grid density (20 million compared to 5 million elements).

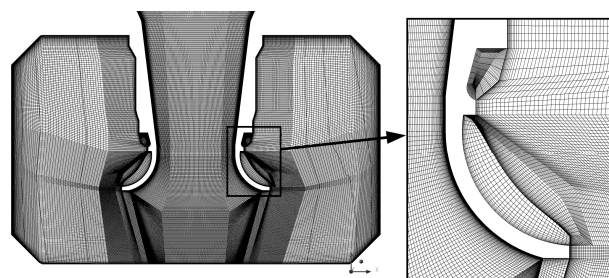


Fig. 2. Cross-section through the computational mesh at Y-plane.

The height of the first row of elements near the floor, below the pump bell is $0.0011D$, and $0.0015D$ elsewhere in the channel. At the pump bell's inner surface the height of the first row of elements is $0.00028D$ at the bell mouth

and $6.6 \cdot 10^{-5} D$ at the narrowest part of the bell. All the previously mentioned dimensions of the first row of elements are of the same order as in [5].

The highest y^+ , in a range between 10 and 100, was observed at the floor at the vortex core. At the bottom side of the pump bell the y^+ values were in the range from 3 to 10, while for the rest of the inner walls of the column they were mostly from 1 to 3.

4. DESCRIPTION OF THE COMPUTATIONS

The computations required a lot of computational resources. The computations began with the commercial code Ansys CFX 11.0. After the release of a new version, 12.0.1, the investigation continued with newly added turbulence models and some additional options for them, like the curvature-correction option. For illustration purposes, the LES computation needed approximately 47 days of computation on 80 computer cores. The whole computation matrix for the comparison of the turbulence models can be found in Table 2.

Table 2. Computation matrix. In case of transient computations time steps were counted from the end of the initial (steady state) computations. Iterations and time steps were rounded to 100.

Simulation number	Simulation name	Turbulence model	Stationary (S) or Transient (T)	ANSYS CFX version used	Initial conditions from:	Iterations (Time steps)
1	SSTstac	SST-2003	S	11.0	- (new)	8600
2	SSTtrans	SST-2003	T	11.0	SSTstac	16600
3	SST-CC	SST-2003 with curvature correction	T	12.0.1	SSTstac	16400
4	SAS	SAS-SST 2005	T	11.0	SSTstac	14500
5	SAS2007	SAS-SST 2007	T	12.0.1	SSTstac	16800
6	SAS-CC	SAS-SST 2005 with curvature correction	T	12.0.1	SSTstac	16600
7	RSMstac	SSG RSM	S	11.0	- (new)	7100
8	RSMtrans	SSG RSM	T	11.0	SSG RSMstac	10700
9	EARSMstac	BSL EARSM	S	12.0.1	- (new)	10000
10	EARSMtrans	BSL EARSM	T	12.0.1	EARSMstac	15600
11	DES	DES-SST	T	12.0.1	SSTstac	16500
12	LES	LES Smagorinsky	T	11.0	SSTstac	20600

The computations were made in the LSC Adria supercomputing center located at Turboinštitut, which consists of 256 IBM HS22 blade servers, each equipped with two quad-core Intel Xeon processors L5530 2.4GHz 8MB L2 and 16 GB RAM. For fast inter-node communication an Infiniband link with the MPI protocol is used.

It was decided to use the SST version described in [9], the SAS-SST, BSL EARSM, SSG RSM developed in [25], and the DES-SST and LES Smagorinsky turbulence models. Since the SAS-SST model was modified in the last CFX version, the versions 2005 ([20]) and 2007 ([21]) were both tested. The BSL EARSM is based on the Hellsten form [26] of the Wallin and Johansson [27] EARSM model. Additionally, since the SST model is an isotropic one and is, as such, insensitive to streamline curvature, this can lead to an over-prediction of the turbulent mixing and to a strong decay of the vortex core. Two computations, SST-CC and SAS-CC, were made with the curvature-correction option, which is based on [15], with a scaling coefficient set to 1.

The results of the steady-state computations were taken as the initial values for the transient runs, as noted in Table 2. In this way the time necessary for the transient computations was shortened, since the computation from the zero velocity field in the fluid would take an enormous computation time with a computational mesh of this size. The use of the thus specified initial values may from time to time impose the wrong results on the transient runs, as we observed in our day-to-day practical work on the water-turbine computations. However, these wrong results are always a consequence of the implied large backflow at the outlet surface of the draft tube for the initial condition, which the next computation cannot then dampen out. Also, since the steady SST computation could not predict the vortex rope in the pump-bell area, it was quite suitable for the initial condition for the other, more accurate, turbulence models. For the SSG RSM transient computation the result of the SSG RSM steady-state computation was taken as the initial condition, and for the EARSM transient computation the EARSM steady-state result was used as the initial condition.

At the inlet boundary conditions the mass flow rates were specified and at the outlet the average static pressure condition was set. Accurate LES computations require a precedent computation of the inlet conditions, for which several computational methods exist, as thoroughly described and compared in [28]. Although these techniques are the only correct methods for a LES computation, Schlüter et al. [29] have shown that for a strongly swirling flow in a combustion chamber the results obtained from quasi-laminar, inlet boundary conditions are comparable to correctly modelled LES computations and measurements, due to high levels of turbulence production in the mixing region, which causes the flow to be independent of the inlet condition. In the current study such a region occurs below and around the suction bell. Since any modelling without a proper pre-computation of the inlet boundary conditions is a speculation, and the LES is not the turbulence model one would choose for the predictions of the industrial pump sumps, it was regarded more as a guideline in our study, despite some comparisons with it (it should also be kept in mind that the LES simulation has already produced good results in [5] with the same time-step size, approximately the same element size at boundary surfaces, and a 1.5-times coarser mesh in each direction). On the other hand, it seemed very important to concentrate on the outlet, since an outlet that is too close to the vortex can significantly affect the results. Therefore, the outlet was moved far downstream from the outlet pipe.

As in [5], the time step for the transient computations was set to $0.002D/U_0$, where U_0 is the mean velocity inside the pump column at the outlet location. Combined with the mesh, this resulted in a maximum Courant number of approximately 10, while the RMS Courant number was around 0.3. The physical time scale for the steady-state computations was set to $0.02D/U_0$.

All the steady-state calculations were stopped long after the convergence was stabilized at some value. In fact, the residuals were oscillating around some value – for the SST computation the RMS velocity residuals were oscillating between $4.82 \cdot 10^{-5}$ and $2.4 \cdot 10^{-4}$, for the EARSM computation between $3.1 \cdot 10^{-5}$ and $5.9 \cdot 10^{-5}$ and for the SSG RSM between $3.7 \cdot 10^{-5}$ and $6.8 \cdot 10^{-5}$. At the moment the computation was stopped the final RMS velocity residual for the SST steady-state run was $1.4 \cdot 10^{-4}$, for the EARSM steady-state run $3.1 \cdot 10^{-5}$, and for the SSG RSM steady-state run $5.1 \cdot 10^{-5}$.

For the transient runs two conditions were set: first, that at each physical time step the RMS velocity residuals should be smaller than 10^{-5} , and a second one, that the number of such loop iterations should be less than or equal to nine. The last condition was applicable for the RSM and EARSM runs, as they both reached nine loop iterations per time step, the SSG RSM by the end of the computation and EARSM even at the beginning of the computation. Instead of 10^{-5} the RSM velocity residuals for the SSG RSM transient run reached values up to $6.75 \cdot 10^{-5}$, and for the EARSM transient run up to $7.8 \cdot 10^{-5}$.

The statistical averaging began at the beginning of the transient runs. For the LES computation the shape of the vortex was fully developed after 500 time steps. Although it would be better to start averaging after 500 time steps of the computation, it is estimated that such an error is not important for the overall estimation of the results. It may have influenced the maximal values of the statistically averaged variables, but to a lesser extent the general picture of the averaged values.

Automatic wall functions were used for all the computations except for the SSG RSM model, where scalable wall functions [30] were used. Automatic wall functions switch from the wall-function solution to the low-Reynolds solution (integration to the wall), depending on the resolution of the local mesh.

An upwind advection scheme based on the use of Barth and Jespersen's limiter [31] (which limits the numerical advection correction in order to suppress possible oscillations due to large gradients) was used for all the computations except for the LES, where the central-difference scheme was used.

5. COMPARISON OF THE COMPUTATION TIME

In order to compare the CPU times of the different turbulence models a set of 100 time-step, transient-case computations on 128 computer cores was made, with the previously mentioned conditions of the RMS velocity residuals and the number of loop iterations per time step. This time the ANSYS CFX 12.0.1 code was used for all the computations. The initial conditions for the computations were the transient final results of the respective turbulence model in Table 2. The only exception was the BSL EARSM, for which the values were measured from time step 7432 to 7531.

Since the computational mesh and the time step were the same for all the models in order to eliminate the mesh's influence on the results, the CPU time depended only on the properties of the turbulence model chosen. Of course, the RANS turbulence models require computational meshes at least an order smaller than a true LES simulation, mainly due to the LES mesh restriction for the aspect ratio at the walls. Therefore, the comparison in Fig. 3 is useful, especially for the RANS (including SAS) turbulence models.

As is clear from the position of the SAS, SST and RSM points in Fig. 3, it seems that the computational time was mostly a result of the number of loop iterations needed per time step, and to a lesser extent of the number of equations calculated for the applied turbulence model.

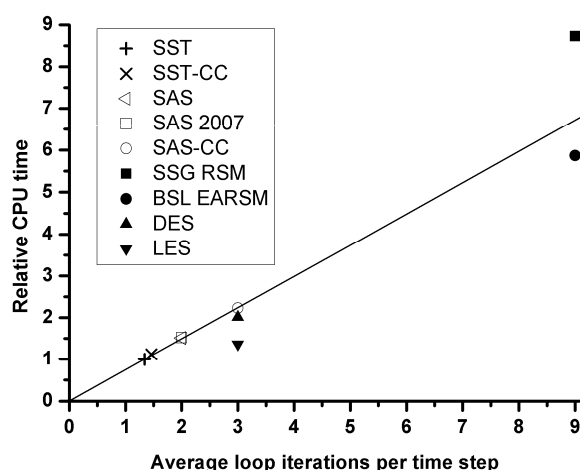


Fig. 3. CPU time comparison for transient simulations. CPU time is relative to SST model CPU time of 100 time steps. Loop iterations per time steps were averaged over 100 time steps. The line goes through the point of the SST simulation result.

The line in Fig. 3 represents the CPU time per loop iteration relative to the SST model: points lying above the line need more CPU time per iteration than the SST model and vice versa. The DES, LES and EARSM models needed less CPU time per iteration than the SST model, whereas the SST and SAS models needed approximately the same CPU time per iteration.

The RSM and EARSM models converge very slowly and the associated relative CPU times were very high, i.e., 8.7 and 5.9, respectively. It seems that from the perspective of CPU time per time step the RSM and EARSM models are not suitable for cases of an industrial pump intake, as the flow phenomena are transient and the required number of time steps might be large.

Although the LES turbulence model needed three loop iterations per time step, it needed almost the same CPU time as the SST model, meaning that it needed less time per iteration than the SST model. However, the LES cannot be used for industrial cases, as discussed previously, since it inherently requires dense computational meshes. Generally, the SST computation is at least an order less expensive than the LES one, since it does not require as fine meshes as the LES turbulence model.

6. COMPARISON OF THE TURBULENCE MODELS

The current study is focused on a simulation of a main submerged vortex. The most interesting quantities are the magnitude of the velocity and the turbulence kinetic energy (TKE). Although the experimental PIV data by Yulin et al. ([6]) included only the two time-averaged, in-plane velocity components, a three-component velocity magnitude is presented in Fig. 4, since the computed two- and three-component, velocity-magnitude results were qualitatively similar. In the studies of Tokyay and Constantinescu ([5] and [24]), the TKE (also denoted as k) for the experimental results was estimated from the in-plane velocity fluctuations u'_{p1} and u'_{p2} using

$$k = \frac{3}{4} \cdot \left(\overline{(u'_{p1})^2} + \overline{(u'_{p2})^2} \right). \quad (3)$$

For the steady-state simulations in Fig. 4 a modelled TKE is drawn, which is based on a solution of a transport equation for the TKE. For transient simulations the sum of the resolved TKE is defined by

$$k = \frac{1}{2} \cdot \left(\overline{(u'_1)^2} + \overline{(u'_2)^2} + \overline{(u'_3)^2} \right), \quad (4)$$

where k is calculated from the resolved time-averaged normal Reynolds stresses, and the time-averaged modelled TKE is represented. The sum of both values is usually called the total TKE. For the LES simulation only the resolved TKE is shown, whereas the modelled part is neglected. In Fig. 6 it is clear that although the TKE values calculated from Eq. 3 and Eq. 4 are not exactly the same, they follow the same pattern. For the simplicity of the comparison the values of TKE calculated using Eq. 4 are shown in Fig. 4, with the range equal to the range used in [5] for the Y -plane. The magnitude of the velocity in Fig. 4 was normalized by U_0 , whereas TKE was normalized by U_0^2 , where U_0 is the mean velocity inside the pump column at the outlet location.

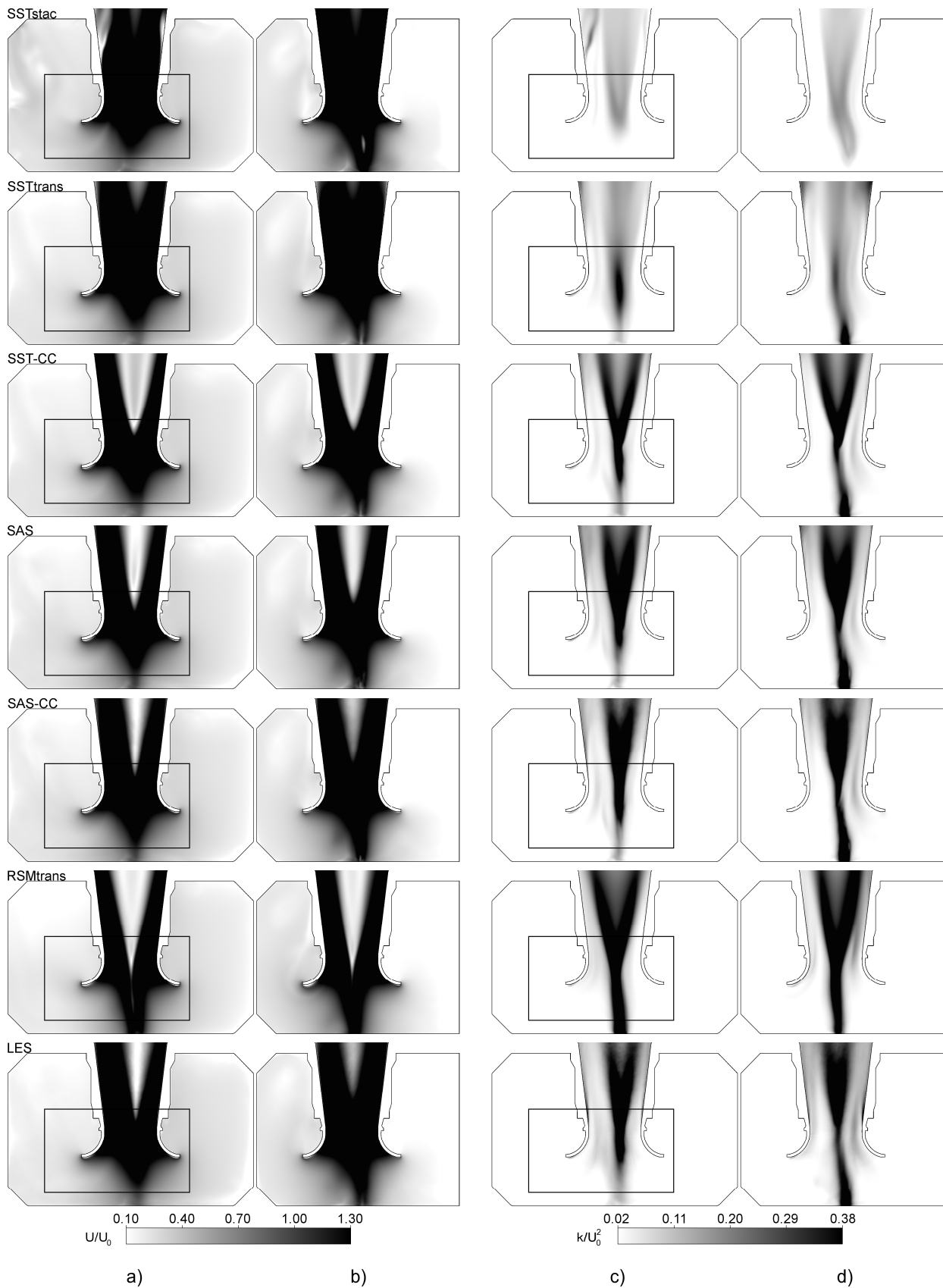


Fig. 4. Comparison of results for different turbulence models: (a) and (b) show velocity magnitude in *Y*- and *X*-plane; (c) and (d) show TKE magnitude in *Y*- and *X*-plane. Black rectangles in (a) and (c) represent the measurement windows; see the top row of Fig. 9a and Fig. 9b, respectively.

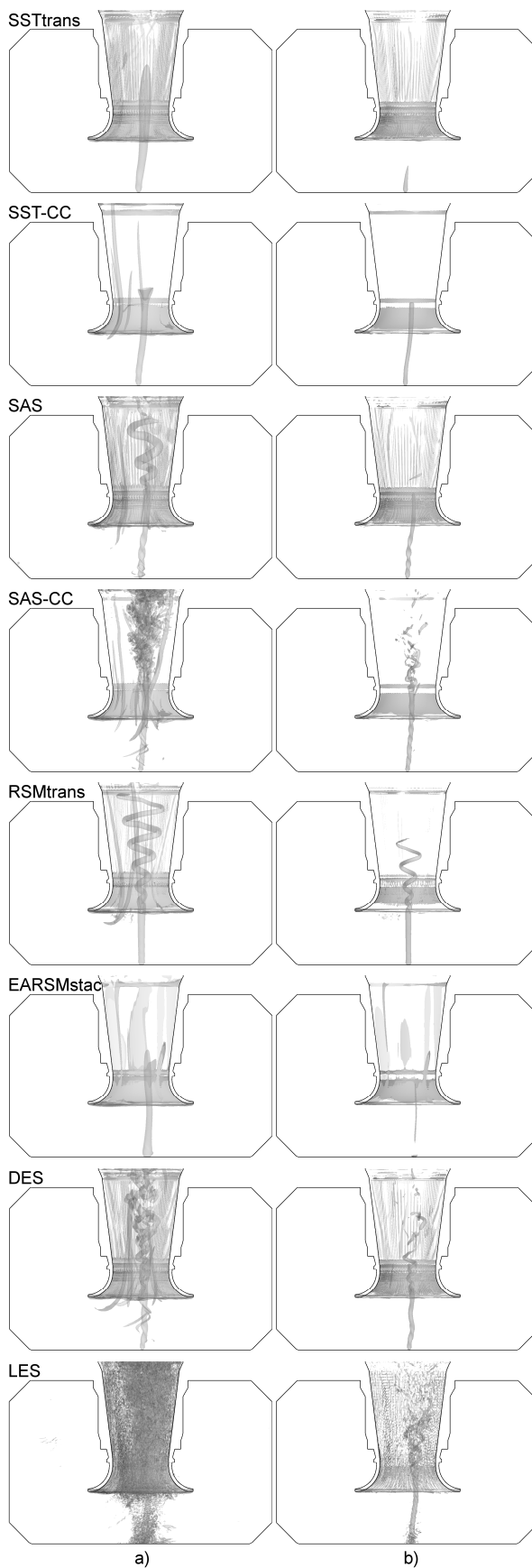


Fig. 5. Comparison of Q iso-surfaces for different turbulence models: a) at $Q=50000 \text{ s}^{-2}$; b) at $Q=500000 \text{ s}^{-2}$. Viewed towards the inlet channels.

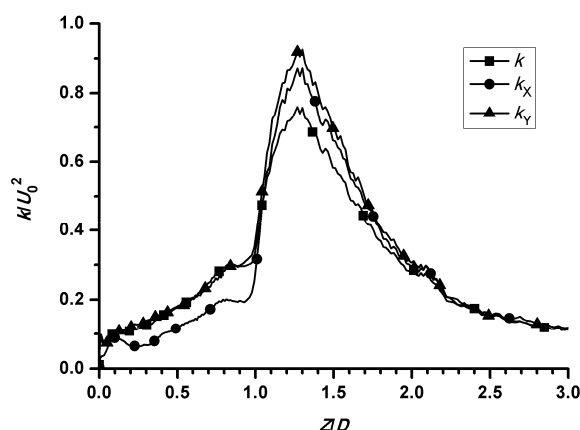


Fig. 6. Turbulence kinetic energy comparison for the LES simulation at a centerline through the pump column. The turbulence kinetic energy k is calculated using Eq. (4), whereas the k_x and k_y are calculated by Eq. (3) from in-plane velocity fluctuations in the X- and Y-plane, respectively.

In Fig. 4 the EARSM, SAS-2007 and DES results are not shown because of space limitations. The DES result is quite similar to the LES or SAS-CC result, whereas the EARSM result is similar to the SST result. The SAS2007 result is almost identical to the SAS2005 result (denoted as SAS in Fig. 4).

All the turbulence models predict approximately the same shape for the velocity-magnitude distribution (Fig. 4a and b). In contrast to [5], even the steady SST computation predicted similar velocity-magnitude values below the pump-bell level as the LES and the experiment (Fig. 9a, top row). However, compared to the LES, the V-shape of the lower velocity magnitudes in the upper region of the vortex (in the pump column) seem to be better predicted with any other turbulence model than with the SST turbulence model.

In [5], the TKE of the steady SST computation produced an annulus-like area of higher TKE values in the pump column at an approximate diameter of $0.5D$, and such TKE values did not reach the floor. It is our assumption that the reason for this was a too coarse mesh in the pump-bell region, since our simulations show better qualitative agreement of the SST model (Fig. 4c and 4d, top frame), as the high TKE values are located on the pipe centerline and extend to the floor.

The steady-state simulations, especially the SST (Fig. 4) and BSL EARSM models (not shown), predicted too low TKE values compared to the LES computation and to the experiment (Fig 9b), due to the unsteady nature of the flow. Compared to the LES result, the unsteady simulations agree much better than the steady ones. Nevertheless, the SST transient simulation predicts lower TKE values than the LES (Fig. 5). It seems that for the prediction of such vortices it is much better to use either the curvature-correction option for the SST model, or any of the SAS models.

In our day-to-day computations the vortical structures are usually represented by the Q-criterion method of vortex identification at a certain time-step (Fig. 5). The Q-criterion [32] is a simple method, applicable for incompressible flows, defined with

$$Q = \frac{1}{2} (\|\boldsymbol{\Omega}\|^2 - \|\mathbf{S}\|^2) > 0, \quad (5)$$

where Q is the second invariant of the velocity gradient tensor, $\boldsymbol{\Omega}$ is the vorticity tensor and \mathbf{S} is the strain-rate tensor. Vortical structures are found by looking for a positive value of Q , indicating that locally the strength of the rotation prevails over the strain rate.

The LES model predicted the shape of the vortex, called the vortex rope, which may occur in the diffuser part of a water turbine under part loads. From Fig. 5 it is clear that the SAS-CC and DES vortex-rope shapes are in best agreement with the LES result. The SST and BSL EARSM models failed to predict the vortex rope. The SST-CC predicted the shape of the bottom part of the vortex much better than the SST model, although it failed to predict the vortex rope. All the SAS models and SSG RSM predicted a vortex rope (Fig 5a). However, at a value of the Q-criterion in Fig 5b it was predicted only by the SAS-CC, SSG RSM, DES and LES.

From the comparison of the magnitude of the maximal velocity and the maximal TKE in Plane 1 and on Line 1 (see Fig. 1b), which is not shown because of space limitations, it was concluded that in general the relative velocity gradients are not as high as the relative TKE gradients. Therefore, the averaging time plays an important role in the comparison of the TKE inside the vortex between the measurements and the CFD simulation, as the vortex meanders and the averaged TKE values become smeared. For comparison: the highest measured TKE value on Line 1, as published [5], is approximately $0.32k/U_0^2$ (also in Fig. 9b, top row), whereas in our LES simulation the value is $0.14k/U_0^2$ on Line 1 and $1.33k/U_0^2$ in Plane 1. The result is probably indicating that the averaging time of the LES simulation should be longer. Therefore, in the second part of the study a longer simulation with the selected turbulence model (SAS CC) was made.

The slope of a curve of a scaled time-averaged absolute circulation in the Z-direction inside the pump column (Fig. 7) can be used as a measure of the swirling decay in a pipe (Fig. 7). The circulation was calculated by using Stokes' theorem as a surface integral of absolute vorticity in the Z-direction, scaled by U_0 and D . It is clear that most of the transient simulations follow the curve of the LES result. The SST-model steady-state simulation predicted a too large circulation at the pump-bell inlet, and also a slightly slower decay rate than the LES simulation. A slower decay rate was also found in the case of the SST transient simulation between $Z=1D$ and $Z=1.75D$. The SSG RSM turbulence-model simulation predicted a slightly lower swirl intensity at the bell-mouth inlet and a slightly higher decay rate between $Z=1.5D$ and $Z=2.2D$ than the LES simulation. This may be either due to the different initial result or due to the differences in the turbulence models. A jump in circulation Γ at a Z/D value of 2 is due to the diffuser expansion.

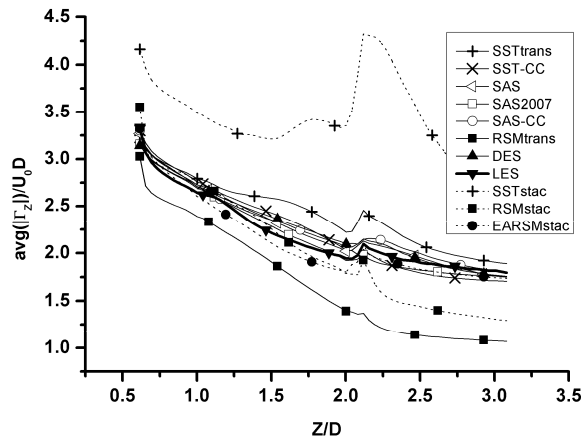


Fig. 7. Comparison of scaled time-averaged circulation Γ in Z-direction inside pump column. Dotted lines represent steady-state simulations. Line of LES simulation is heavier for comparison purposes.

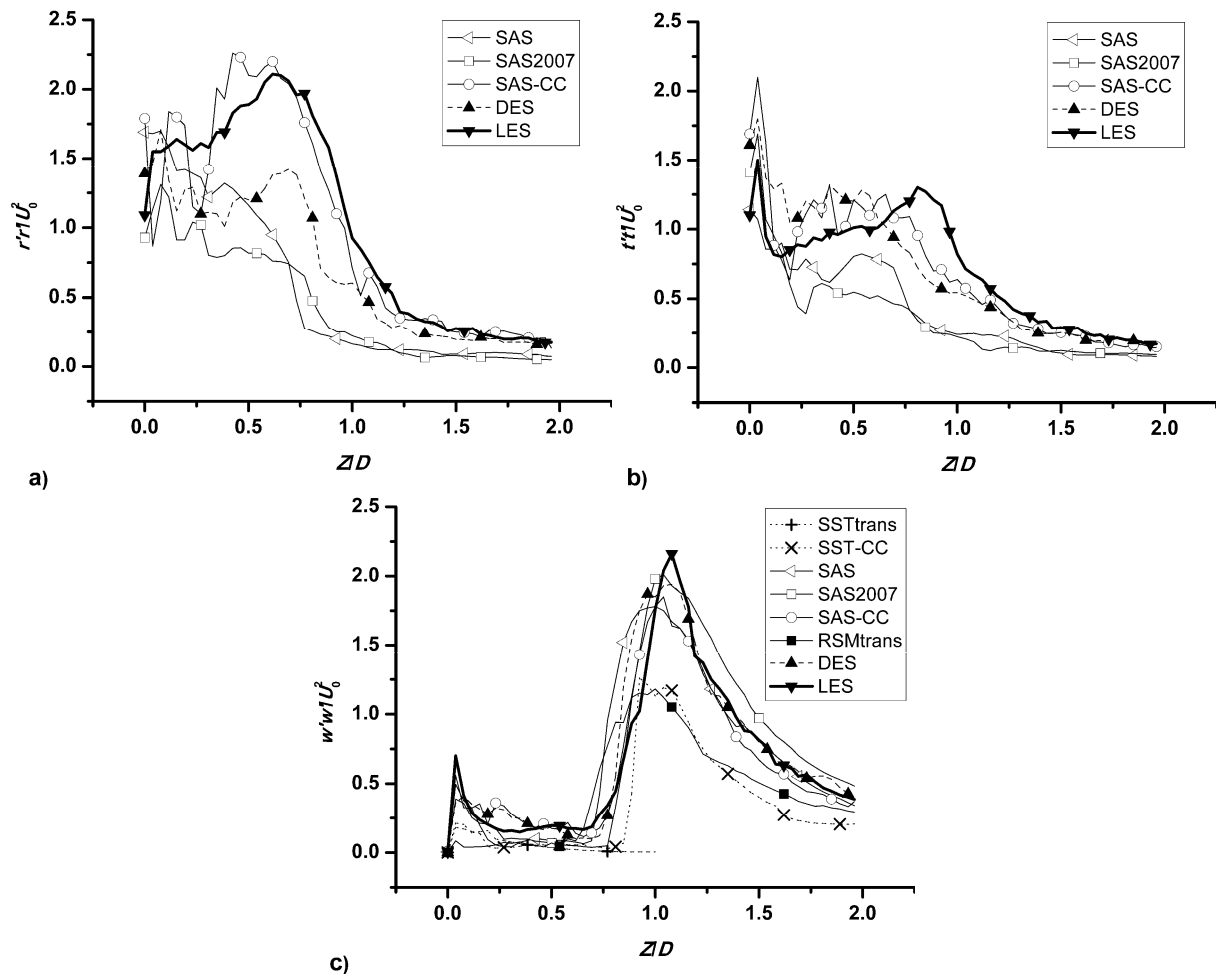


Fig. 8. Scaled Reynolds stresses at maximal total TKE points inside pump column for transient simulations. Line of LES simulation is heavier for comparison purposes.

In Fig. 8 the Reynolds stresses are compared. Since the averaging for our simulations may not have been long enough, as discussed in the previous paragraph, and since the computational time for the simulations was long (approximately 1 month per simulation), the Reynolds stresses shown are lying on the averaged center of the vortex instead of lying on the pump-column centerline. In this way we have avoided the differences that have occurred due to the different "average" vortex position in the simulations, either due to a too short averaging time or due to the differences in the turbulence models. The "averaged" vortex position was defined using the points with the highest total TKE, one per each Z-plane slice. Of course, such points are distributed differently for different simulations. To make the comparison easier the Reynolds stresses are transformed into a locally rotated Cartesian coordinate system.

From Fig. 8 it can be seen that the SAS-CC and DES agree relatively well with the LES simulation results. The SST-CC predicts lower values of the Reynolds stresses in the Z-direction (Fig. 8c). The SST simulation completely failed, and the values for the Reynolds stresses are shown only up to a Z height of $1D$. Namely, as the main vortex was not strong enough, the highest total TKE points above the Z value of $1D$ were lying close to the pump-column wall due to another vortex being sucked from the flow, and not in the central vortex area, due to the main vortex. For all the shear Reynolds stresses the SAS-based simulations agree relatively well with the LES simulation.

7. FINAL COMPARISON WITH THE MEASUREMENT DATA

For the second part of the study it was decided to do a longer computation with a chosen turbulence model and to compare it with the measurement data. If the findings of the previous results and the facts about the turbulence models are recapitulated it is easier to decide for such a model. First of all, the flows inside the pump sump and the vortex itself have a transient nature, so the flow should be computed as a transient simulation. Therefore, in the subsequent text only the transient results will be discussed. The RSM models, including the algebraic ones, seem not to be suitable due to the considerably longer CPU time compared to all the other treated models. The SST and SST-CC models could not predict the vortex rope. The DES model uses a LES inside the main computational domain and therefore encounters the same problem as the LES: if the time step is too high the results would fail as the predicted eddy viscosity would be too low [23]. Therefore, it would be better to use one of the SAS models instead of the DES, as the SAS has a solid theoretical background and is scale adaptive, meaning that at too large time steps the eddy viscosity adapts (increases). The SAS-CC model predicted a result very similar to the LES result when comparing the shape of the vortex rope, much closer than the SAS2005 and SAS2007 models. For all the reasons described it was decided to use the SAS-CC model as the final one, although it needed one iteration per time step more than the SAS models.

In order to speed up the final computation it was decided to shorten the inlet channels and to simulate the channels separately. For the channel simulation a length of 100 channel diagonals was used. The computational mesh had the same density as the original mesh, so the channel mesh consisted of 22 million elements (23.5 million nodes). The channels were simulated by a SST model. The outlet velocities, k and ϵ were used as the inlet boundary conditions for the pump sump.

The simulated length of the shortened pump sump was approximately the same as in [5], $7.4D$. The mesh was also made a bit sparser at the inlet and outlet sections where the SAS term of the SAS model is not important. Thus, the final computational mesh consisted of 25 million elements (25.2 million nodes).

The final simulation of the pump sump was made using the SAS2007 turbulence model with a CC option. For the initial solution the SAS-CC result (Table 2) was used. The new statistics began after time step 500 and lasted for another 75,000 time steps, as in [5].

In Fig. 9 and Fig. 10 the final results (the bottom rows of Fig. 9 and Fig. 10) are compared to the experimental data (top rows of Fig. 9 and Fig. 10), published in the study of Tokyay and Constantinescu [5]. In Fig. 9 the result shows a relatively good, qualitative agreement with the experimental data, whereas in Fig. 10 a good quantitative agreement is observed. As the result captures all the important trends it can be concluded that the SAS-CC turbulence model can be used for the simulation of the pump intakes.

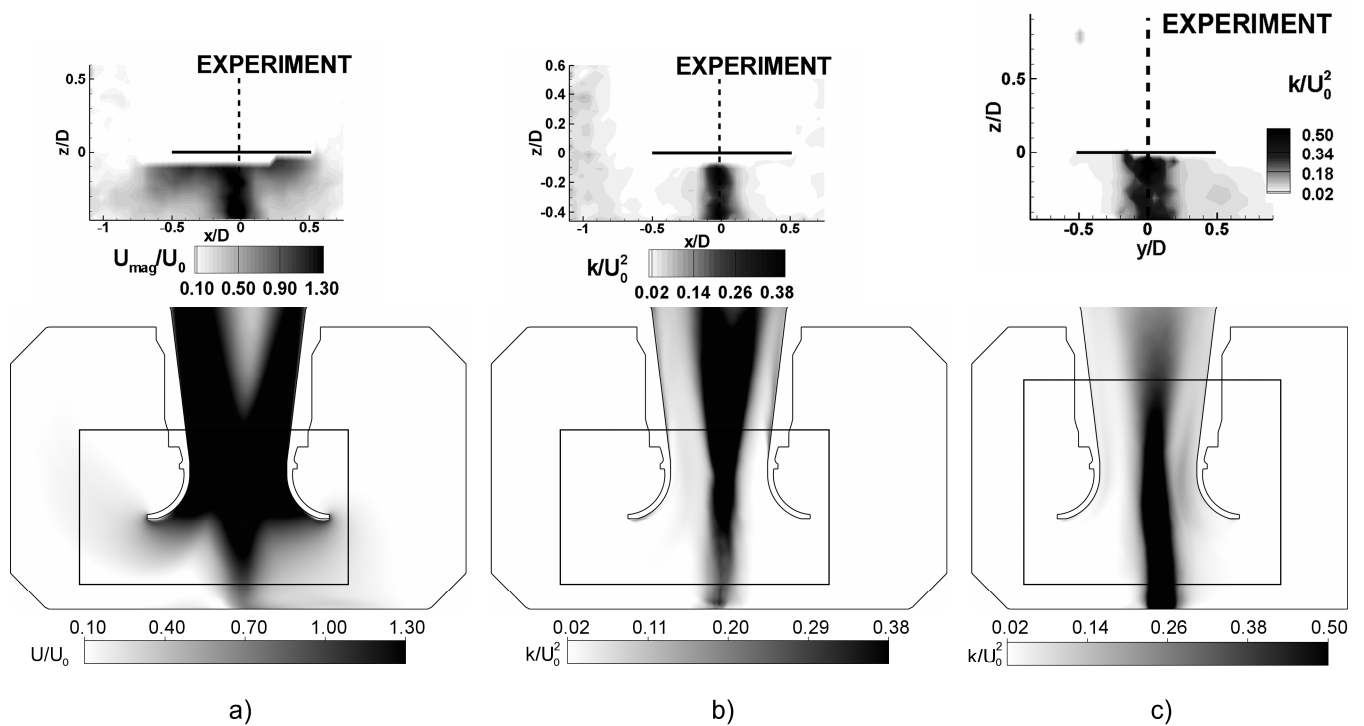


Fig. 9. Comparison of SAS-CC results (bottom row) with experiment (top row): a) velocity magnitude in Y-plane; b) total TKE in Y-plane; c) total TKE in X-plane. Black rectangles in bottom row represent the measurement windows (top row). The experimental results are from a study of Tokyay and Constantinescu [5] (with permission from ASCE), measured by Yulin et al. [6].

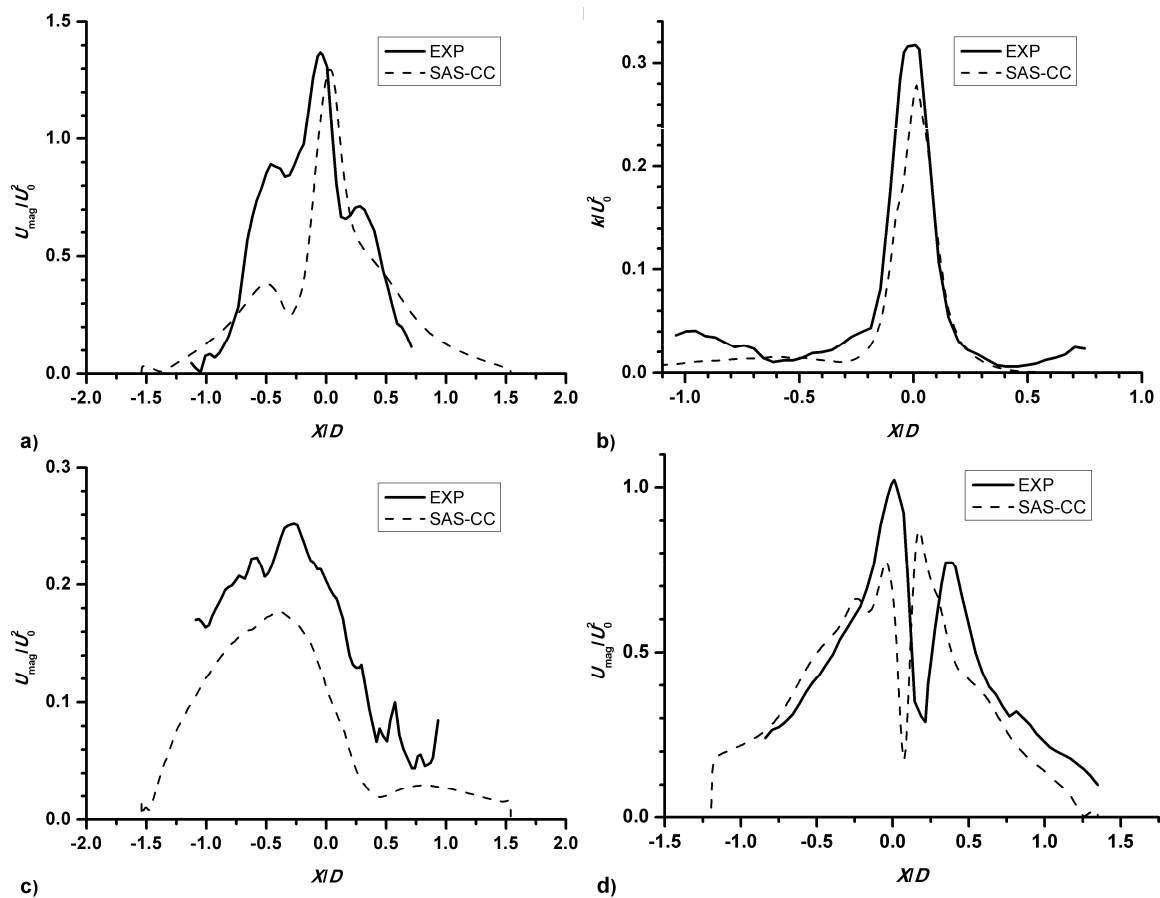


Fig. 10. Comparison of SAS-CC results with experiment: a) velocity magnitude in Y-plane at $Z=0.35D$ (Line 2); b) total TKE in Y-plane at $Z=0.17D$ (Line 1); c) velocity magnitude in Y2-plane at $Z=0.35D$ (Line 3); d) velocity magnitude in Plane 2 at $X/D=0$ (Line 4). The experimental results are from a study of Tokyay and Constantinescu [5] (with permission from ASCE), measured by Yulin et al. [6].

8. CONCLUSIONS

Transient phenomena in the pump intake were simulated with different turbulence models in order to decide for a model that is suitable for industrial pump-sump cases from the perspective of accuracy and, partially, also the CPU time. In the first part of the study eleven simulations were compared with the LES simulation and with the published study of Tokyay and Constantinescu (2006).

The first part answered many questions regarding the choice of the turbulence model. Namely, all the turbulence models, including the SST, have predicted the appearance of a vortex. The predicted TKE of all the steady-state simulations was too low since the simulated phenomena are transient.

For the unsteady simulations, the SST model may produce misleading results in terms of a quantitative assessment of TKE and regarding the Q-criterion of the vortex identification. It is advisable to use the curvature-correction option as the TKE and Q-criterion agreement with the LES results was much better and the CPU time increase was negligible.

In the case of fine computational meshes in the pump-bell region it is quite tempting to use one of the SAS models, as they managed to capture the existence of the vortex rope, besides the generally good agreement with the LES in all quantities. Again, it is advisable to use the curvature-correction option.

The BSL EARSIM and SSG RSM models needed a lot of CPU time, as they converged relatively slowly compared to the other models. Therefore, it is advisable to use them on coarser meshes. Although the EARSIM model started to diverge, the results before the noticed flow anomalies were quite similar to the SST model results.

The DES-SST model produced results similar to the LES. Since the DES can produce misleading results when used with a too large time step and since it needed just a little less CPU time than the SAS-CC, we suggest using the latter one for industrial cases instead.

The best-practices guidelines for strongly swirling flows say that two-equation turbulence models cannot properly describe the flow, whereas the RSM models give much better results, at least regarding the mean velocity and pressure. Even for the RSM and algebraic RSM models the discrepancy in the turbulence predictions can be large. The observed case in this paper has confirmed that two-equation models, such as the SST model, under-predict the vortex itself and the turbulence kinetic energy. The RSM model has shown great improvement over the SST model, but it seems much better to use the CC option with the two-equation models than the full RSM models, as the computational time for the RSM is at least three times larger than for the SST-CC or SAS-CC models due to larger time per iteration and due to a slower convergence.

In the second part of the study a longer simulation with the SAS-CC turbulence model was made. The comparison with the experimental values showed relatively good qualitative and quantitative agreement, meaning that the SAS turbulence model with the curvature-correction option can be used for industrial pump-sump cases.

In the current study the results were obtained on a very fine mesh (and with small time steps) so that the time needed for the computations was relatively large. It is expected that by using a slightly coarser mesh (for instance, as in [5]) and allowing the use of wall functions, the SAS-CC turbulence model should produce results of the same accuracy as the LES simulation on an order-of-magnitude finer grid. By using such a mesh the SAS-CC turbulence model can be applicable to the pump-sump industrial cases, even without a supercomputer.

ACKNOWLEDGEMENTS

The research was partially funded by the Slovenian Research Agency ARRS - Contract No. 1000-09-160263.

REFERENCES

- [1] **ANSI/HI 9.8**. American National Standard for Pump Intake Design. Hydraulic Institute, Parsippany, New Jersey, 1998.
- [2] **Constantinescu, G. S., and Patel, V. C.** Numerical Model for Simulation of Pump-Intake Flow and Vortices. *J. Hydr. Engrg.*, 1998, **124**(2), 123-134.
- [3] **Rajendran, V. P., Constantinescu, G. S., and Patel, V. C.** Experimental Validation of Numerical Model of Flow in Pump-Intake Bays. *J. Hydr. Engrg.*, 1998, **125**(11), 1119-1125.
- [4] **Constantinescu, G. S., and Patel, V. C.** Role of Turbulence Model in Prediction of Pump-Bay Vortices. *J. Hydr. Engrg.*, 2000, **126**(5), 387-392.
- [5] **Tokyay, T. E., and Constantinescu, S. G.** Validation of a Large-Eddy Simulation Model to Simulate Flow in Pump Intakes of Realistic Geometry. *J. Hydr. Engrg.*, ASCE, 2006, **132**(12), 1303-1315.
- [6] **Yulin, W., Yong, L., and Xiaoming, L.** PIV Experiments on Flow in a Model Pump Suction Sump. *Research Report*, Tsinghua Univ., Tsinghu, China, 2000.
- [7] **Škerlavaj, A., Vehar, F., Pavlin, R., and Lipej, A.** A Hydraulic Study of Cooling Water Intake Structure. In Proc., Int. Meeting of the Workgroup on Cavitation and Dynamic Problems in Hydraulic Machinery and Systems, IAHR, Brno, 2009, pp. 143-153.
- [8] **Ansys.** *Ansys CFX-Solver Theory Guide, Release 12.0*. Ansys, Inc., Canonsburg, PA, 2009.

- [9] **Menter, F. R., Kuntz, M., and Langtry, R.** Ten Years of Industrial Experience with the SST Turbulence Model. *Turbulence, Heat and Mass Transfer 4*, K. Hanjalic, Y. Nagano, and M. Tummers, eds., Begell House, Inc., NY (USA), Wallingford (UK), 2003, 625–632.
- [10] **Hadžić, I., Hadžić, H., and Muzaferija, S.** CASE 9.2: Periodic flow over a 2-D hill - Description of numerical aspects and turbulence models. In 9th IAHR/ERCOFTAC Workshop on Refined Turbulence Modelling, Darmstadt, Germany, 2001.
- [11] **Skoda, R., and Schilling, R.** Computation of the Test Case 9.2: Periodic flow over a 2D hill. In 9th IAHR/ERCOFTAC Workshop on Refined Turbulence Modelling, Darmstadt, Germany, 2001.
- [12] **Hellsten, A.** Description of the Computations for the Test Case 9.2. In 9th IAHR/ERCOFTAC Workshop on Refined Turbulence Modelling, Darmstadt, Germany, 2001.
- [13] **Jang, Y. J., Temmerman, L., and Leschziner, M. A.** Investigation of Anisotropy-Resolving Turbulence Models by Reference to Highly-Resolved LES Data For Separated Flow. In Proc., ECCOMAS CFD Conf. Swansea, Wales, UK, 2001.
- [14] **Hellsten, A., and Wallin, S.** Explicit algebraic Reynolds stress and non-linear eddy-viscosity models. *Int. J. Comput. Fluid D.*, 2009, **23**(4), 349–361.
- [15] **Spalart, P.R., and Shur, M.** On the sensitization of turbulence models to rotation and curvature. *Aerospace Sci. Tech.*, 1997, **1**(5), 297–302.
- [16] **Smirnov, P. E., and Menter, F. R.** Sensitization of the SST Turbulence Model to Rotation and Curvature by Applying the Spalart-Shur Correction Term. *J. Turbomachinery*, 2009, **131**(4), 041010.1–041010.8.
- [17] **Fröhlich, J., and Terzi, D.** Hybrid LES/RANS Methods for the Simulation of Turbulent Flows. *Progr. Aersp. Sci.*, 2008, **44**, 349–377.
- [18] **Spalart, P. R., Jou, W.-H., Strelets, M. and Allmaras, S.R.** Comments on the feasibility of LES for wings, and on a hybrid RANS/LES approach, In Advances in DNS/LES, Proc. of 1st AFOSR Int. Conf. On DNS/LES, Ruston, Louisiana. C. Liu, Z. Liu and L. Sakell, eds., Greyden Press, Columbus, OH, 1997.
- [19] **Spalart, P. R., Deck, S., Shur, M. L., Squires, K. D., Strelets, M. Kh., and Travin, A.** A new version of detached-eddy simulation, resistant to ambiguous grid densities. *Theor. Comput. Fluid Dyn.*, 2006, **20**, 181–195.
- [20] **Menter, F.R., and Egorov, Y.** A Scale-Adaptive Simulation Model using Two-Equation Models. In Proc., 43rd Aerospace Sciences Meeting and Exhibit, Reno NV, AIAA Paper 2005–1095.
- [21] **Egorov, Y., and Menter, F.** Development and Application of SST-SAS Turbulence Model in the DESIDER Project. In Advances in Hybrid RANS-LES Modelling. Notes on Numerical Fluid Mechanics and Multidisciplinary Design, 2008, 97, pp. 261–270 (Springer Berlin / Heidelberg).
- [22] **Davidson, L.** Evaluation Of The SST-SAS Model: Channel Flow, Asymmetric Diffuser And Axi-Symmetric Hill. In Proc., ECCOMAS CFD Conf. TU Delft, The Netherlands, 2006.
- [23] **Menter, F.R., and Egorov, Y.** The Scale-Adaptive Simulation Method for Unsteady Turbulent Flow Predictions. Part 1: Theory and Model Description. *Flow, Turbulence and Combustion*, 2010, **85**(1), 113–138.
- [24] **Tokyay, T. E., and Constantinescu, S. G.** Investigation of Flow Physics of Pump Intake Flows Using Large Eddy Simulation. *IIHR Technical Report*, Univ. of Iowa, Iowa, 2005, <http://www.iihr.uiowa.edu/products/pubvid/pdf/IIHR445.pdf>.
- [25] **Speziale, C. G., Sarkar, S., and Gatski, T. B.** Modelling the pressure-strain correlation of turbulence: an invariant dynamical systems approach. *J. Fluid Mech.*, 1991, **277**, 245–272.
- [26] **Hellsten, A.** New advanced turbulence model for high-lift aerodynamics. In Proc., 42nd Aerospace Sciences Meeting and Exhibit, Reno NV, AIAA Paper 2004–1120.
- [27] **Wallin, S., and Johansson, A.** A complete explicit algebraic Reynolds stress model for incompressible and compressible flows. *J. Fluid Mech.*, 2000, **403**, 89–132.
- [28] **Tabor, G. R., Baba-Ahmadi, M. H., de Villiers, E., and Weller, H. G.** Construction of Inlet Conditions for LES of Turbulent Channel Flow. In Proceedings of ECCOMAS 2004, Jyväskylä, 24–28 July 2004.
- [29] **Schlüter, J. U., Pitsch H., and Moin, P.** Large Eddy Simulation Inflow Conditions for Coupling with Reynolds-Averaged Flow Solvers. *AIAA Journal*, 2004, **42**(3), 478–484.
- [30] **Grotjans, H. and Menter, F.R.** Wall functions for general application CFD codes. In ECCOMAS 98 Proceedings of the Fourth European Computational Fluid Dynamics Conference, 1998, pp. 1112–1117.
- [31] **Barth, T.J., and Jespersen, D.C** The Design and Application of Upwind Schemes on Unstructured Meshes. *AIAA Paper* 89-0366, 1989.
- [32] **Hunt, J. C. R., Wray, A. A., and Moin, P.** Eddies, stream, and convergence zones in turbulent flows. In Proceedings of the Summer Program, Center for Turbulence Research, 1988, pp. 193–208.

APPENDIX

Notation

D = diameter of pump column above the surface level;

k = turbulence kinetic energy;

The final, definitive version of this paper has been published in *Proceedings of the Institution of Mechanical Engineers, Part A: Journal of Power and Energy*, 225(6), 764–778, September 2011 by SAGE Publications Ltd, All rights reserved. © A. Škerlavaj, L. Škerget, J. Ravnik and A. Lipej.
<http://online.sagepub.com>, DOI: 10.1177/0957650911403870

k_i = turbulence kinetic energy, calculated from in-plane velocity fluctuations at a plane normal to i direction;

r = radial velocity in rotated Cartesian coordinate system;

Q = second invariant of velocity gradient tensor;

\mathbf{S} = strain rate tensor;

t = tangential velocity in rotated Cartesian coordinate system;

U_0 = mean velocity in the pump column above the surface level;

U = velocity magnitude;

\mathbf{u} = velocity vector;

u_i = velocity component in the i direction;

u_{pi} = velocity component in the in-plane i direction;

u' = velocity fluctuation;

w = velocity in Z direction;

X = X Cartesian coordinate;

Y = Y Cartesian coordinate;

Z = Z Cartesian coordinate;

Γ = circulation;

$\mathbf{\Omega}$ = vorticity tensor;

ν = kinematic viscosity; and

ρ = density.